International Journal of Nanoscience
Vol. 17, No. 3 (2018) 1850013 (9 pages)

DOI: 10.1142/S0219581X18500138

Optical and Electronic Analysis of Pure and Fe-Doped ZnO Thin Films Using Spectroscopic Ellipsometry and Kramers–Kronig Method

Maryam Motallebi Aghgonbad* and Hassan Sedghi†
Department of Physics, Faculty of Science
Urmia University, Urmia, Iran
**m.motallebi89@gmail.com*
†*H.sedghi@urmia.ac.ir*

Received 19 September 2017
Accepted 5 December 2017
Published 17 January 2018

In the present work, pure and Fe-doped ZnO thin films were deposited on glass substrates by sol–gel method. Zinc acetate and iron nitrate were used as the starting material and dopant source, respectively. The concentration of Fe doping was 6 at.% and 8 at.%. The optical and electronic properties of pure and Fe-doped ZnO thin films such as refraction index, extinction coefficient, dielectric function and optical band gap energy of the layers were obtained by spectroscopic ellipsometry method in the wavelength range of 300–900 nm. The incidence angle of the layers kept 70°. Also data obtained by Kramers–Kronig relations were used for comparison. The influence of Fe-doping concentration on the optical and electronic properties of thin films was studied. The transmittance data of ZnO thin films showed that 6 at.% Fe-doped ZnO thin film has the highest transmittance value. Dielectric function of pure ZnO films was found to be higher compared with Fe-doped ones. Also it can be deduced from the results that Fe doping influences the optical band gap energy of thin films.

Keywords: Fe-doped ZnO; spectroscopic ellipsometry; Kramers–Kronig; sol–gel; optical band gap.

1. Introduction

Semiconducting devices are mostly based on advancement of thin film technology. Thin film is a two-dimensional material deposited by either atom-by-atom or molecule-by-molecule condensation method.[1] Zinc oxide (ZnO) is a II–VI compound semiconductor with a wide direct band gap of 3.37 eV at room temperature.[2] Physical properties of ZnO depend on growth method, environmental conditions, doping concentration, temperature and the crystal structure.

Transition metal ions are considered as a most important activator to enhance the optical and electronic properties.[3] Ti, Fe and Co are 3d transition metals which are noticed as effective dopants of ZnO for optoelectronic applications. Among these, Fe-doped ZnO thin films have wide applications in the field of optics and microelectronics.

*Corresponding author.

Due to application of Fe-doped ZnO thin films in magnetoelectronic devices, these films are widely investigated but there was little attention to their optical and electronic properties. Recently, Fe-doped ZnO thin films get more attention due to their tunable optical band gap properties.[4] ZnO thin films have been grown by a variety of techniques such as magnetron sputtering,[5,6] pulsed laser deposition,[7] spray pyrolysis,[8,9] evaporation,[10] chemical vapor deposition,[11] molecular beam epitaxy,[12] and sol–gel processing.[1,13–15] Sol–gel method has many advantages such as low cost, simple deposition procedures, no need of vacuum deposition conditions, easier fabrication of large-area film, easier control of composition and being able to deposit thin films on complex-shaped substrates.[16] However, the possibility of practical application of any semiconductor lies on the effective manipulation of its physical properties. An effective method for manipulating the physical properties of semiconductors involves impurity doping.[17] Doped ZnO thin films have been extensively studied because of its various properties such as ultraviolet photo detectors, gas sensors,[18] thin film transistors,[19] optoelectronics[20] and solar cells.[21] The effect of Fe doping in ZnO on glass substrate has become a topic of numerous scientific investigations.[22–25] From the ellipsometry spectra of the samples, one can find out the optical properties of the films.

In this work, pure and Fe-doped ZnO thin films were prepared on glass substrates by spin coating method. Optical and electronic properties of the Fe-doped ZnO thin films as a function of Fe concentration were examined. In particular, spectroscopic ellipsometry (SE) has been widely used to investigate the physical properties of ZnO thin films in a broad spectral range. Spectroscopic ellipsometric measurement and Kramers–Kronig (KK) method were used to calculate the optical and electronic properties of the layers. The effect of Fe doping concentration on optical and electronic properties of ZnO thin films was investigated.

2. Experimental Details

Pure and Fe-doped ZnO thin films were coated on glass substrates by sol–gel spin coating method. Zinc acetate dehydrate ($Zn(CH_3COO)_2 \cdot 2H_2O$), iron nitrate ($Fe(NO_3)_3 \cdot 9H_2O$), 2-methoxyethanol and monoethanolamine (MEA) were used as the precursor, dopant source, solvent and stabilizer, respectively. First, zinc acetate was dissolved in 2-methoxyethanol. The solution was stirred at 60°C for an hour. During the stirring, MEA was added to it drop by drop until a clear solution was formed. The concentration of zinc acetate was 0.25 M, and the molar ratio of MEA to zinc acetate was fixed at 1. For doped films, iron nitrate was added to the mixture with concentration of 6 at.% and 8 at.%. The solution was aged for 72 h at room temperature. Before deposition, the substrates were cleaned thoroughly. The films were deposited on glass substrates with the spin coating speed of 4800 rpm. The samples were preheated in air for 10 min at 200°C to evaporate the solvent and remove the organic residuals. Then the films were annealed at 500°C for an hour. The optical and electronic properties of pure and Fe-doped ZnO thin films were obtained by SE method. Also KK relations were used to calculate optical and electronic properties of the films. These two methods were compared with each other.

When ZnO thin film is formed on the glass substrate, the effect of backside reflection leads to complications in the SE analysis. To eliminate the backside reflection, in measuring the properties of Fe-doped ZnO thin films, the rear surface of the substrates was roughened and Scotch tape was used during the measurement. In this case, when light enters the Scotch tape, scattering by the cloudy translucent material and backside reflections are suppressed.

3. Results and Discussion

3.1. *SE method*

Ellipsometry is an indirect optical technique in that information about the physical properties of a sample is obtained through modeling analysis. In this work, SE is used to extract the ellipsometry parameters, psi (ψ) and delta (Δ), which were defined from the ratio of the amplitude reflection coefficient for p and s polarizations:

$$\rho \equiv \tan\,\psi\,\exp(i\Delta) \equiv \frac{r_p}{r_s}. \tag{1}$$

The incidence angle of 70° was used. The sample model used to analyze the ellipsometry data is shown in Fig. 1.

This model consists of a glass substrate, pure or Fe-doped ZnO layer, surface roughness and air as the ambient medium. Surface roughness layer was modeled by effective medium approximation with 50% of voids and 50% of Fe-doped ZnO.

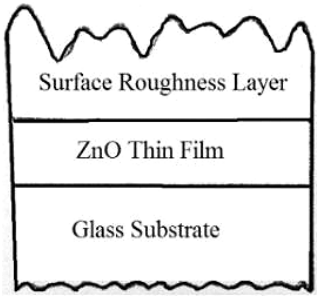

Fig. 1. Optical model used to analyze the ellipsometry data.

In Figs. 2–4, the experimental and fitted ellipsometric parameters (ψ, Δ) is shown for pure and Fe-doped ZnO layer as a function of wavelength.

The mean square error (MSE) is used to qualify the difference between the experimental and fitted data:

$$(\mathrm{MSE})\chi^2 = \frac{1}{N}\sum_{i=1}^{N}\frac{(\mathrm{Mes}_i - \mathrm{Th}_i)^2}{\sigma_i^2}, \qquad (2)$$

where σ_i is the standard deviation of the ith data point, N is the number of data points, Mes_i is the ith experimental data point and Th_i is the ith

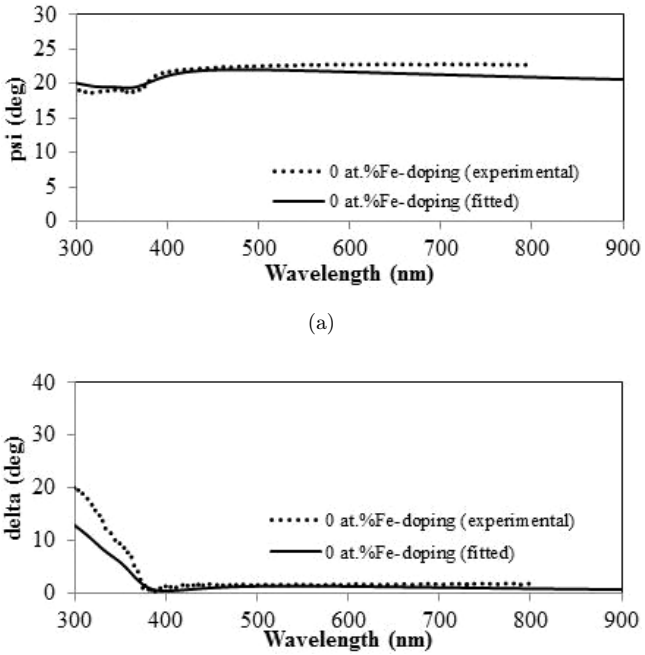

Fig. 2. The experimental and fitted ellipsometry parameters: (a) ψ and (b) Δ, as a function of wavelength for pure ZnO thin films.

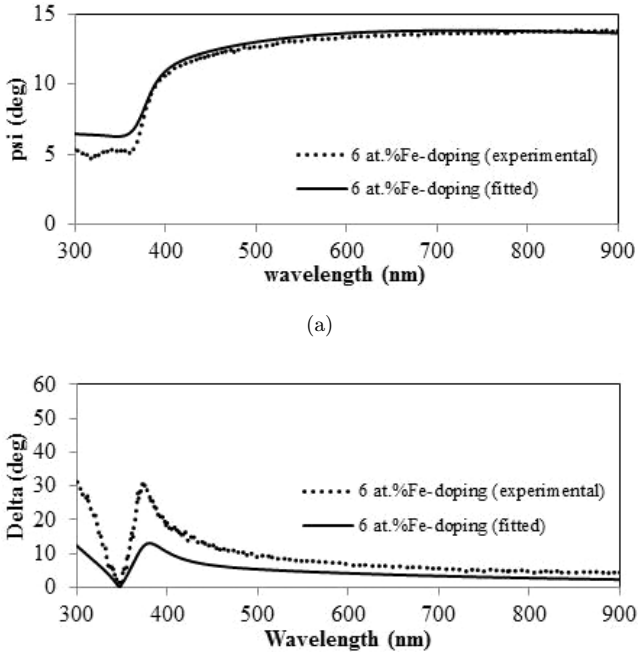

Fig. 3. The experimental and fitted ellipsometry parameters: (a) ψ and (b) Δ, as a function of wavelength for Fe-doped ZnO thin films with atomic percentages of 6 at.%.

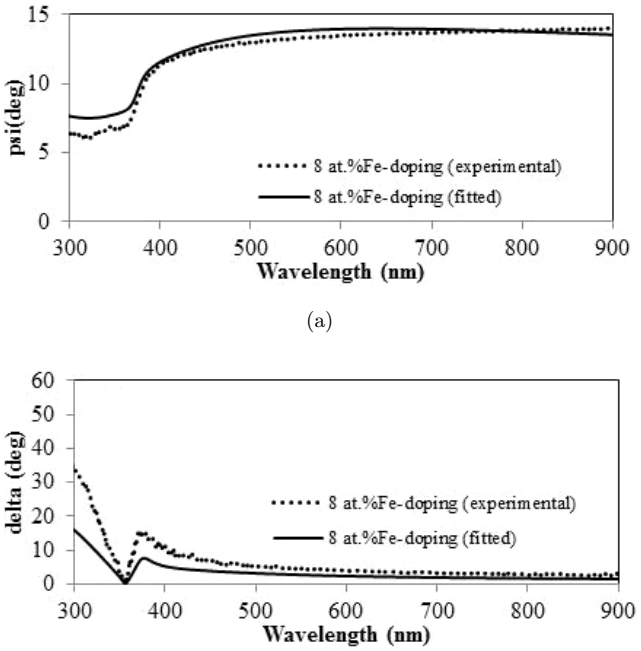

Fig. 4. The experimental and fitted ellipsometry parameters: (a) ψ and (b) Δ, as a function of wavelength for Fe-doped ZnO thin films with atomic percentages of 8 at.%.

calculated data point from assumed theoretical model. When the model matches the experimental data as closely as possible, the MSE exhibits a minimum value.

Table 1 shows the MSE obtained by spectroscopic ellipsometric method for pure and Fe-doped ZnO thin films. From MSE data in Table 1, it can be deduced that the optical model matches the experimental data. Adding surface roughness layer in the model gives a significant improvement to the MSE value compared with the single layer model.

The optical transmittance of pure and Fe-doped ZnO thin films in the wavelength range of 300–900 nm is shown in Fig. 5. Fe incorporation influences the transmittance in the visible range. The lowest transmittance is observed for pure ZnO thin films. By addition of Fe dopant to the layers, the transmittance spectra are increased. By increasing wavelength, there is an increasing trend for transmittance of layers. This shows that in the visible spectral range the layers get transparent.

In Fig. 6 the real part of refractive index and the imaginary part (the extinction coefficient) of pure and Fe-doped ZnO thin films are shown. It can be deduced from Fig. 6(a) that for all layers there is a peak at about 380 nm wavelength. Around that wavelength, in Fig. 6(b), the extinction coefficient decreases which shows an interband transition. In the visible spectral range, the magnitude of extinction coefficient is very small.

Table 1. MSE obtained by spectroscopic ellipsometric method for the pure and doped ZnO thin films.

Sample	Fe doping concentration (at.%)	Mean square error
I	0	0.6551
II	6	0.7377
II	8	0.6528

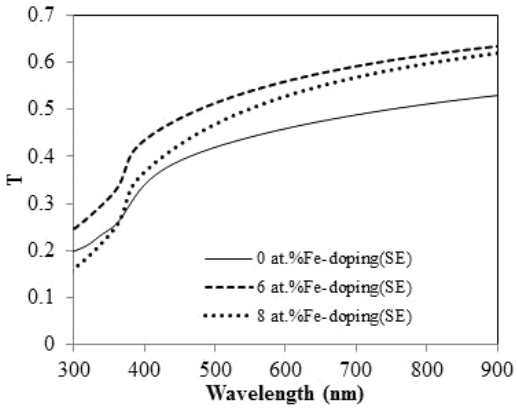

Fig. 5. Transmittance spectra of pure and Fe-doped ZnO thin films as a function of wavelength.

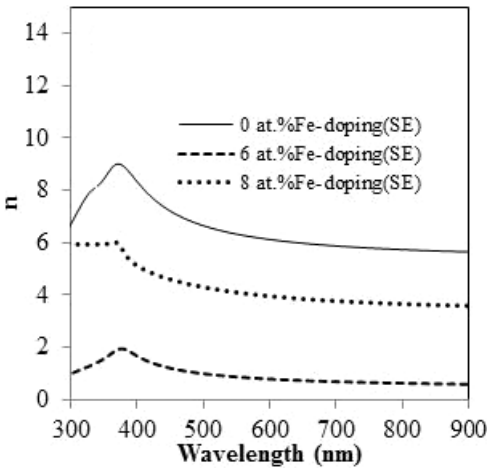

(a)

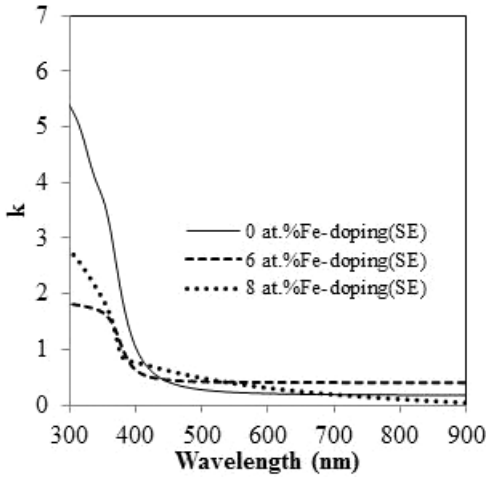

(b)

Fig. 6. (a) The refractive index and (b) extinction coefficient of pure and doped ZnO thin films obtained by the SE method.

Figure 7 shows the real and imaginary parts of dielectric function obtained by the SE method. Both real and imaginary parts of dielectric function have higher value in pure ZnO thin films compared with Fe-doped ones.

It is known that the absorption coefficient near the band edge shows an exponential dependence on photon energy:

$$\alpha(\lambda) = \alpha_0 \exp\left(\frac{h\nu}{E_0}\right). \quad (3)$$

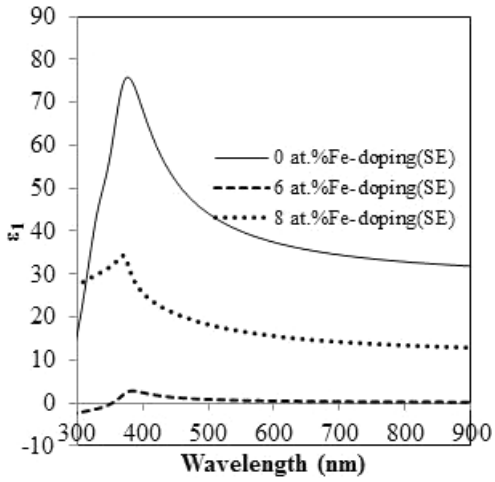

(a)

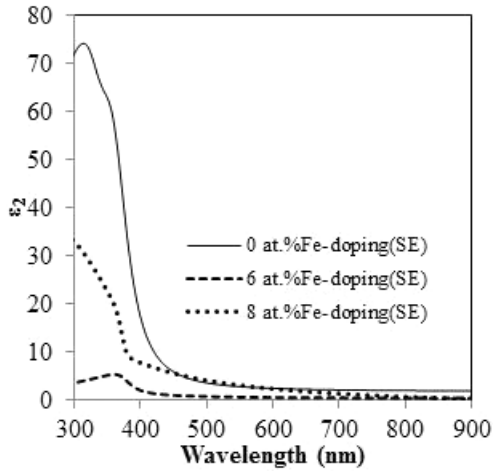

(b)

Fig. 7. (a) Real and (b) imaginary parts of dielectric function of pure and doped ZnO thin films obtained by the SE method.

As we know, incidence of a photon with energy of $h\nu$ on a semiconductor leads to a transition between the highest occupied state of valance band and the lowest unoccupied state of the conduction band. This phenomenon is applied to calculate the optical band gap energy of ZnO thin films using Tauc relation.[26] In Fe-doped ZnO thin films, the optical band gap energy mainly depends on the valance state of Fe ions.[27] In Fe-doped ZnO thin films, there is a large variability in the optical behavior which leads to inconsistent conclusions. By addition of Fe into ZnO films, maximum of valence band is increased and the minimum of conduction band is decreased which leads to the reduction of band gap. In contrast, substituting Fe^{3+} ions into Zn^{2+} leads to providing extra free carrier concentrations. As a result, the Fermi level moves toward the conduction band and the band gap increases.[28] This makes the optical band gap of Fe-doped ZnO thin films tunable.

The optical band gap energy was determined by applying the Tauc relation[29] as given below:

$$\alpha h\nu = A(h\nu - E_g)^n, \tag{4}$$

where α is the absorption coefficient, $h\nu$ is the photon energy and A is a constant. Due to the direct E_g for ZnO thin films, $n = 1/2$ is more suitable.

Considering Fe-doped thin films, it can be seen from Fig. 8 and Table 2 that the optical band gap increased with the increasing Fe-doping concentration from 6 at.% to 8 at.%.

An extrapolation of the linear region of a plot of $(\alpha h\nu)^2$ on the Y-axis versus photon energy $(h\nu)$ on

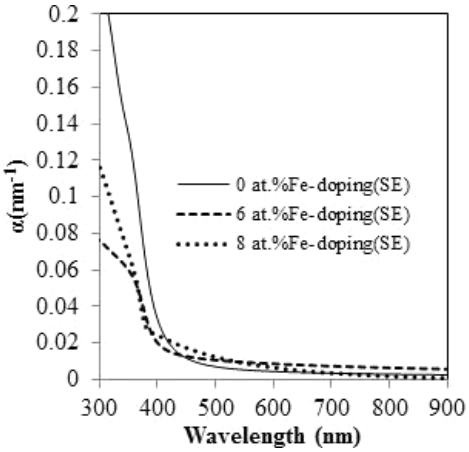

(a)

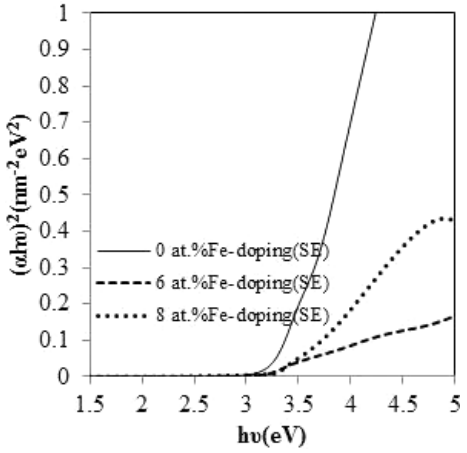

(b)

Fig. 8. (a) Absorption coefficient and (b) $(\alpha h\nu)^2$ versus $h\nu$ of pure and doped ZnO thin films obtained by SE method.

Table 2. The optical band gap energy of pure and doped ZnO thin films obtained by the SE method.

Fe doping concentration (at.%)	BG (eV) SE method	Fe doping, Ref. 14 (at.%)	BG (eV), Ref. 14
0	3.4	0	3.305
6	3.2	3	3.320
8	3.5	5	3.322

the X-axis gives the value of the optical band gap (E_g).

In Fig. 8, the absorption coefficient and also $(\alpha h\nu)^2$ versus $h\nu$, which is known as Tauc plot, for pure and Fe-doped ZnO thin films are shown.

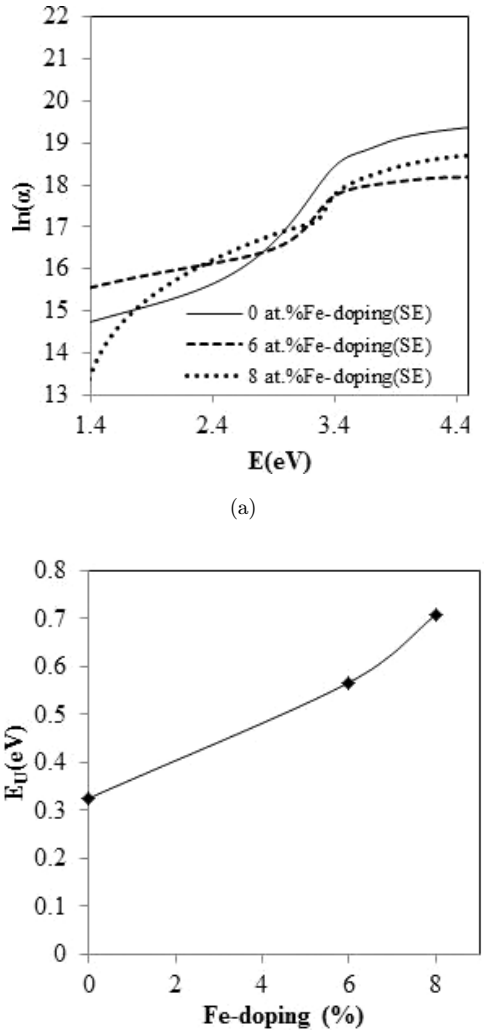

(a)

(b)

Fig. 9. (a) $\ln(\alpha)$ versus photon energy of ZnO thin films and (b) Urbach energy for ZnO thin films versus Fe-doping concentrations.

Table 2 shows the calculated optical band gap of the layers.

Figure 9 shows the plot of $\ln(\alpha)$ versus photon energy of ZnO thin films and the obtained Urbach energy for ZnO thin films with different Fe-doping concentrations, respectively.

The imperfection in the structurally disordered film leads to broadening the bands of localized states. As mentioned, near the band edge, the absorption coefficient has an exponential dependence on photon energy. This dependence is given as follows:

$$\alpha = \alpha_0 \exp\left(\frac{h\nu}{E_u}\right), \tag{5}$$

where α_0 is a constant and E_u is the Urbach energy. Urbach energy is the width of the tails of the localized states associated with the amorphous state in the forbidden band. As it can be seen by increasing Fe-doping concentration, Urblach energy of the films increases. It means that by adding Fe dopants, ZnO thin films become less crystalline.

3.2. *KK method*

In this work also, KK relations were used to calculate the optical properties of pure and doped ZnO thin films.

To calculate the phase angle $\theta(E)$, the following relation is used[30–32]:

$$\theta(E) = \frac{E}{\pi}\int_0^{E_2} \frac{\ln R(E) - \ln R(E_0)}{E^2 - E_0^2}\mathrm{d}E + \frac{1}{2\pi}\ln\left[\frac{R(E)}{R(E_2)}\right]\ln\frac{E_2 + E}{|E_2 - E|} + \frac{1}{\pi}\sum_0^{\infty}\left[4\left(\frac{E}{E_2}\right)^{2n+1}\right](2n+1), \tag{6}$$

where E denotes the photon energy, E_2 the asymptotic limitation of the free-electron energy and $R(E)$ the reflectance. Hence, if E_2 is known, then $\theta(E)$ can be calculated.

Figure 10 shows the optical reflectance of pure and Fe-doped ZnO films versus energy.

It can be deduced from Fig. 10 that pure ZnO thin films have the highest reflectance; by Fe-doping, the reflectance of the layers decreases.

Then the real and imaginary parts of the refractive index were calculated by the following

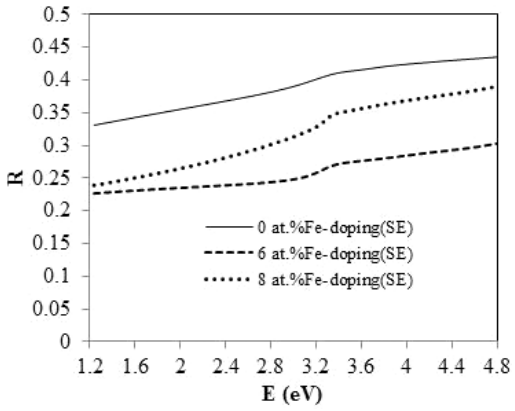

Fig. 10. Reflecance spectra of pure and Fe-doped ZnO thin films as a function of wavelength.

equations:

$$n = \frac{1-R}{1+R-2\sqrt{R}\cos\theta}, \tag{7}$$

$$k = \frac{2\sqrt{R}\sin\theta}{1+R-2\sqrt{R}\cos\theta}. \tag{8}$$

Figure 11 shows the real and imaginary parts of refractive index by the KK method. The low extinction coefficient value in the visible region indicates the better quality of the film. In Fig. 12, the real and imaginary parts of dielectric function are obtained by:

$$\varepsilon_1 = n^2 - k^2, \tag{9}$$

$$\varepsilon_2 = 2nk, \tag{10}$$

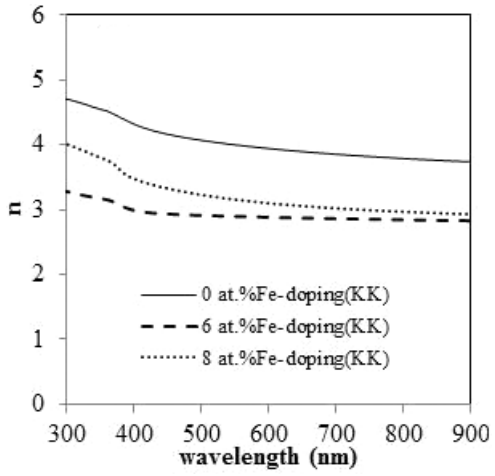

(a)

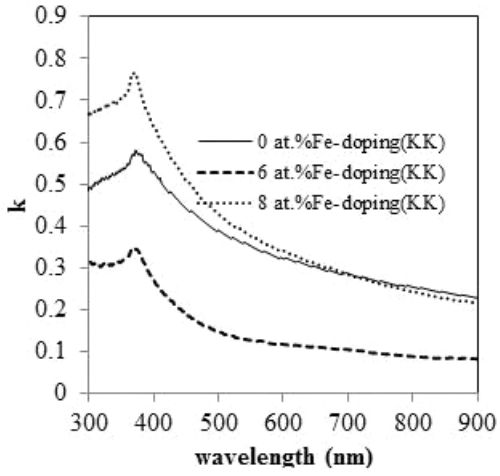

(b)

Fig. 11. (a) The refractive index and (b) extinction coefficient of pure and doped ZnO thin films obtained by KK method.

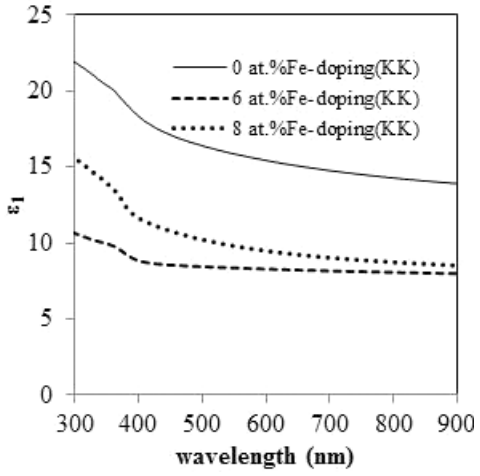

(a)

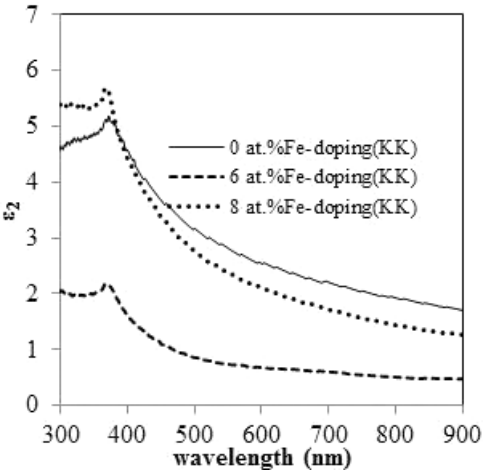

(b)

Fig. 12. (a) Real and (b) imaginary parts of dielectric function of pure and doped ZnO thin films obtained by KK method.

in which n and k are the real and imaginary parts of refractive index. In pure ZnO thin films, both real and imaginary parts of dielectric function are higher compared with doped ones.

Figure 13 shows the absorption coefficient and $(\alpha h\nu)^2$ versus $h\nu$ for the layers. The absorption coefficient is calculated by the following equation:

$$\alpha = \frac{4\pi k}{\lambda}, \tag{11}$$

where k is the extinction coefficient and λ is the wavelength.

In Fe-doped ZnO thin films, the absorption coefficient shows an increase with Fe-doping concentration. The way that the optical band gap can be obtained is discussed in previous session. The results for band gap energy of the layers by KK method are shown in Table 3.

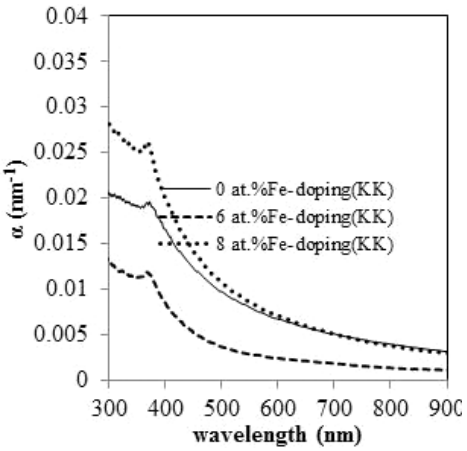

(a)

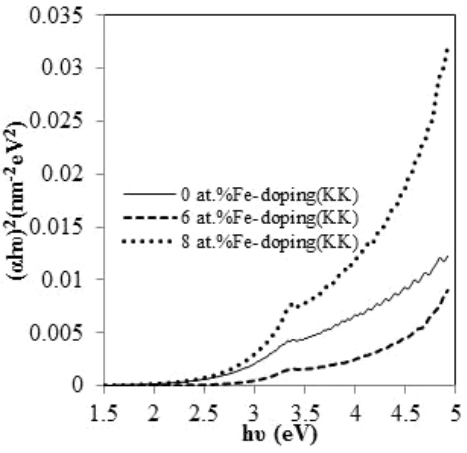

(b)

Fig. 13. The absorption coefficient and $(\alpha h\nu)^2$ versus $h\nu$ of pure and doped ZnO thin films obtained by KK method.

Table 3. The optical band gap energy of pure and doped ZnO thin films obtained by KK method.

Sample	Fe doping concentration (at.%)	Band gap energy (eV), KK method
I	0	2.8
II	6	3.7
II	8	3.5

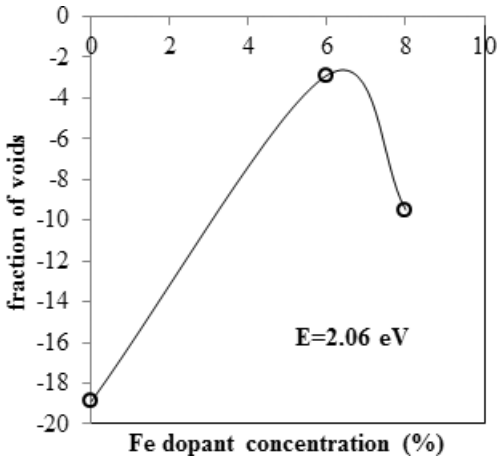

Fig. 14. Fraction of voids versus Fe dopant concentration in ZnO thin films.

The valence state of Fe is an important factor in optical properties of ZnO thin films. Fe dopants in ZnO thin films can be in two forms of Fe^{2+} or Fe^{3+}, or even coexistence of these two forms is seen. As a result, the optical properties of Fe-doped ZnO thin films are complex that was discussed in Sec. 3.1.

The void fraction of pure and Fe-doped ZnO thin films at $E = 2.06\,\text{eV}$ is shown in Fig. 14. It can be seen that with changing of Fe concentration, the fraction of voids changes too.

4. Conclusion

The optical properties of pure and Fe-doped ZnO films were studied with respect to iron concentration in the starting solution, in which the iron nitrate was used as a Fe source. The optical properties were discussed in two different methods: SE and KK relations. The lowest transmittance was observed for pure ZnO thin film. In the visible spectral range, the extinction coefficient of all layers was very small, which shows the high transparency of ZnO thin films. The optical band gap energies of pure and Fe-doped ZnO thin films were calculated

between 3.2 eV and 3.5 eV in SE, which was obtained between 2.8 eV and 3.7 eV with KK relations. Comparing with previous works, the results obtained by SE are more accurate.

References

1. D. D. Mulmi, A. Dhakal and B. Ram Shah, *Nepal J. Sci. Technol.* **15**, 111 (2014).
2. E. Gungor, T. Gungor, D. Caliskan, A. Ceylan and E. Ozbayb, *Appl. Surf. Sci.* **318**, 309 (2014).
3. K. Verma, B. Chaudhary, V. Kumar, V. Sharma and M. Kumar, *Vacuum* **146**, 524 (2017).
4. N. Srinatha, K. G. M. Nair and B. Angadi, *Adv. Powder Technol.* **28**, 1086 (2017).
5. A. Jain, M. Johari, A. Jain, P. K. Pandey and R. Agrawa, *Int. J. Innov. Res. Sci. Eng. Technol.* **2**, 3144 (2013).
6. S. Y. Choi, K. Choi and S. J. Kim, *Int. J. Adv. Res. Electr. Electron. Instrum. Eng.* **2**, 6034 (2013).
7. K. J. Saji, R. Manoj, R. S. Ajimsha and M. K. Jayaraj, *Advances in Thin-Film Coatings for Optical Applications III*, 62860D (2006).
8. K. Nadarajah, C. Y. Chee and C. Y. Tan, *J. Nanomater.* (2013).
9. Q. G. Al-Zaidi, A. M. Suhail and W. R. Al-Azawi, *Appl. Phys. Res.* **3**, 89 (2011).
10. K. Lim, M. A. Abdul Hamid, R. Shamsudin, N. H. Al-Hardan, I. Mansor and W. Chiu, *Materials* **9**, 1 (2016).
11. S. Vallejos, F. D. Maggio, T. Shujah and C. Blackman, *Chemosensors* **4**, 1 (2016).
12. D. S. Darvish and H. A. Atwater, *J. Cryst. Growth* **319**, 39 (2011).
13. L. Znaidi, T. Touam, D. Vrel, N. Souded, S. Ben Yahia, O. Brinza, A. Fischer and A. Boudrioua, *Acta Phys. Polon. A* **121**, 165 (2012).
14. M. Saleem, L. Fang, H. B. Ruan, F. Wu, Q. L. Huang, C. L. Xu and C. Y. Kong, *Int. J. Phys. Sci.* **7**, 2971 (2012).
15. H. F. Hussein, G. M. Shabeeb and S. Sh. Hashim, *J. Mater. Environ. Sci.* **2**, 423 (2011).
16. L. Xu and X. Li, *J. Cryst. Growth* **312**, 851 (2010).
17. A. Mendoza-Galván, C. Trejo-Cruz, J. Lee, D. Bhattacharyya, J. Metson, P. J. Evans and U. Pal, *J. Appl. Phys.* **99**, 014306 (2006).
18. V. Musat, A. M. Rego, R. Monteiro and E. Fortunato, *Thin Solid Films* **516**, 1512 (2008).
19. H. Lee, X. Zhang, J. Hwang and J. Park, *Materials* **9**, 851 (2016).
20. C. Rameshkumar and R. Subalakshmi, *J. Chem. Pharmaceut. Res.* **7**, 459 (2015).
21. O. Gençyılmaz, F. Atay and I. Akyüz, *J. Clean Energy Technol.* **4**, 90 (2016).
22. K. Singh, D. K. Shukla, S. Majid, R. Dhar, R. J. Choudhary and D. M. Phase, *J. Phys.: Conf. Ser.* **755**, 012040 (2016).
23. S. Y. Al Dabagh and E. E. Makhool, *IOSR J. Dent. Med. Sci.* **15**, 54 (2016).
24. S. M. Salaken, E. Farzana and J. Podder, *J. Semicond.* **34**, 073003 (2013).
25. S. Vasudevan, *J. Chem. Pharmaceut. Sci.* **1**, 42 (2017).
26. P. Ariyakkani, L. Suganya and B. Sundaresan, *J. Alloys Compd.* **695**, 3467 (2017).
27. M. Salem, S. Akir, T. Ghrib, K. Daoudi and M. Gaidi, *J. Alloys Compd.* **685**, 107 (2016).
28. T. Srinivasulu, K. Saritha and K. T. Ramakrishna Reddy, *Modern Electronic Materials* (2017). https://doi.org/10.1016/j.moem.2017.07.001.
29. J. Tauc, R. Grigorovici and A. Vancu, *Phys. Stat. Sol.* **15**, 627 (1966).
30. H. Kangarlou, M. Motallebi Aghgonbad and Z. Barjisi, *Optik* **124**, 107 (2013).
31. H. Kangarlou, M. Motallebi Aghgonbad and A. Abdollahi, *Mater. Sci. Semicond. Process.* **30**, 1 (2015).
32. H. Kangarlou, A. Abdollahi and M. Motallebi Aghgonbad, *Opt. Spectrosc.* **113**, 321 (2012).